THE ASTROPHYSICAL JOURNAL, 342:272–284, 1989 July 1

THE ROTATION CURVE OF THE MILKY WAY TO $2R_0$

MICHEL FICH
University of Waterloo

LEO BLITZ
Institute for Advanced Study; and University of Maryland

AND

ANTONY A. STARK
AT&T Bell Laboratories
Received 1988 September 6; accepted 1988 December 9

ABSTRACT

The rotation curve of the Milky Way is determined for galactocentric distances between 3 kpc and 17 kpc using inner and outer Galaxy data sets and a simple function to represent the data. H I tangent point velocities are used inside the solar circle; CO velocities and spectrophotometric distances of associated H II regions are used in the outer Galaxy. A variety of functional forms for the rotation curve and various assumptions about the velocity field and the objects observed are tested.

Seven of the eight outermost points lie above the mean rotation curve; it has not been possible, however, to produce a simple function that adequately describes this rise and simultaneously matches the data for the rotation curve in the inner Galaxy. The simplest functions tried, linear and power law in velocity versus galactic distance, resulted in a curve that changes in Θ by less than 2% from R_0 to $2R_0$ assuming the IAU standard rotation constants of $R_0 = 8.5$ kpc and $\Theta_0 = 220$ km s^{-1}. With these values for the rotation constants we recommend that a flat curve $\Theta = 220$ km s^{-1} be used for kinematic distance determinations in the outer Galaxy. Recommendations are given of other rotation curve functions for use in modeling the mass distribution of the Galaxy or for determining kinematic distances with other rotation constants.

Subject headings: galaxies: The Galaxy — galaxies: internal motions — interstellar: molecules — radio sources: 21 cm radiation

I. INTRODUCTION

The rotation curve of the Milky Way is fundamental to galactic structure studies. It is the central piece of information on which models of the mass distribution of the Galaxy are built, and it is widely used to determine kinematic distances to objects that have measured radial velocities. Furthermore, study of the noncircular motions within the Galaxy (such as streaming in spiral arms, expansion in shells, and random motions of clouds) first requires recourse to a rotation curve, to enable one to remove the circular motion due to galactic rotation.

In this paper we present a unified analysis of the galactic rotation curve using H I, CO and spectrophotometric data obtained in the northern hemisphere to determine the rotation curve from $R = 3$–17 kpc. We examine a number of different functional forms to fit the data and discuss the errors and uncertainties that go into its determination. We compare our results with nine recent studies of the rotation curve and make specific recommendations on the choice of curves to use for kinematic studies and mass modeling.

II. ANALYSIS

a) Data Base

The principal source of information used for the rotation curve analysis is the catalog of CO velocities of H II regions by Blitz, Fich, and Stark (1982, hereafter BFS). This catalog lists the H II regions seen optically from the northern hemisphere and contains distances determined from optical spectrophotometric methods. These distances were determined by a variety of authors and do not constitute a uniform sample. Table 1 lists the data for the 104 H I regions that have independently determined distances and velocities. The table includes several recent determinations of distances to the exciting stars of H II regions (Chini and Wink 1984; Forbes 1985).

A comparison of distances to objects observed by Chini and Wink (1984) show that the best values from other observers are systematically lower than the Chini and Wink distances by 25%. For the sake of consistency, we have adjusted all the Chini and Wink distances by this factor and estimated the distance uncertainties to each object as follows: the uncertainty in the distance modulus to each star is assumed to be 0.6 mag (= 28%), a value taken from observations of southern hemisphere H II region exciting stars (Brand 1986). We then add a 25% distance uncertainty in quadrature

$$\left(\frac{\Delta d}{d}\right)^2 = \left[\frac{(0.28)^2}{n} + (0.25)^2\right], \qquad (1)$$

where n is the number of observed stars in the H II region.

We have attempted to include only H II regions that are "kinematically distinct." By this we mean that if an H II region complex contains more than one H II region only one is listed in Table 1. The CO velocity is the mean value of the emission for the entire complex. The positions of the H II regions used to compute the rotation curve are shown in Figure 1.

To obtain the rotation curve in the inner Galaxy we use the H I data from Burton and Gordon (1978). This represents the velocities of the "tangent points" which are related geometrically to galactocentric distances in the standard way (e.g.,

TABLE 1

H II Region Data

Object	l (°)	b (°)	distance (kpc)		V_r ($km\,s^{-1}$)		Object	l (°)	b (°)	distance (kpc)		V_r ($km\,s^{-1}$)	
S8	351.36	0.61	1.7	±0.3	-4.3	±1.5	S175	120.36	1.97	1.7	±0.5	-49.6	±0.5
S11	352.80	0.64	1.74	0.3	-3.9	1.0	S177	120.63	-0.14	2.5	0.8	-34.2	0.4
S25	5.95	-1.30	1.8	0.2	12.0	1.5	S184	123.04	-6.32	2.2	0.7	-30.4	1.1
S27	4.24	22.51	0.17	0.05	3.0	1.5	S190	133.71	1.21	2.1	0.2	-46.0	5.3
S45	15.00	-0.68	2.2	0.2	20.0	2.0	S199	138.30	1.56	2.1	0.2	-39.0	1.0
S46	15.42	3.31	2.0	0.7	18.0	1.0	S202	139.99	2.09	0.8	0.3	-11.5	2.0
S48	16.58	-0.35	2.9	0.9	44.6	1.3	S206	150.68	-0.77	3.3	0.8	-22.6	0.5
S49	17.06	0.70	2.2	0.2	24.2	2.0	S208	151.27	1.97	7.6	0.8	-30.2	0.4
S54	18.90	2.09	2.0	0.2	27.6	0.5	S209	151.61	-0.24	8.2	2.4	-52.2	2.4
S65	29.05	-0.76	3.5	1.2	52.4	1.0	S211	154.65	2.46	5.9	1.8	-37.6	0.9
S69	31.83	1.46	3.6	1.2	55.4	1.0	S212	155.39	2.65	6.0	0.6	-35.3	0.3
S74	39.86	-1.23	2.4	0.8	48.1	1.8	S217	159.15	3.27	5.2	0.8	-20.5	1.1
S82	53.56	0.04	1.1	0.4	24.0	1.0	S219	159.36	2.57	4.2	0.6	-24.5	1.2
S86	59.66	-0.21	1.9	0.2	26.8	1.4	S220	160.31	-12.34	0.4	0.04	7.0	3.0
S90	63.12	0.44	4.0	1.3	22.2	1.0	S228	169.19	-0.90	3.5	1.1	-8.7	2.5
S93	64.14	-0.47	3.2	1.1	21.3	1.3	S231	173.47	2.55	2.3	0.7	-18.1	0.9
S97	66.83	0.87	3.9	1.4	21.0	1.0	S232	173.43	3.17	1.0	0.3	-23.0	0.5
S99	70.15	1.71	8.0	2.5	-22.9	2.0	S234	173.48	-0.05	2.3	0.7	-13.4	0.7
S101	71.59	2.76	2.5	0.8	13.7	0.4	S236	173.60	-1.78	3.2	0.3	-7.2	0.5
S104	74.79	0.57	4.4	1.4	0.0	2.0	S237	173.97	0.25	1.8	0.3	-4.3	0.7
S112	83.78	3.28	2.1	0.7	-4.0	2.0	S238	176.24	-20.88	0.15	0.05	8.1	0.9
S117	84.64	0.20	0.8	0.3	0.0	3.0	S241	180.79	4.03	4.7	1.2	-6.5	1.0
S119	87.06	-4.19	0.7	0.25	3.5	1.5	S242	182.36	0.19	2.1	0.7	0.0	0.5
S121	90.23	1.72	4.8	1.4	-60.9	0.5	S247	188.96	0.85	3.5	0.9	2.9	1.2
S124	94.57	-1.45	2.6	0.6	-43.4	1.1	S249	189.45	4.38	1.6	0.5	-5.3	2.6
S125	94.40	-5.57	1.0	0.16	8.0	1.0	S252	189.81	0.33	1.5	0.15	7.5	1.0
S126	96.72	-15.14	0.6	0.2	-0.2	0.4	S253	192.23	3.59	4.4	0.4	14.4	0.5
S127	96.27	2.57	7.3	2.3	-94.7	0.4	S254	192.61	-0.04	2.5	0.4	7.5	0.7
S128	97.56	3.16	6.2	2.3	-72.5	0.4	S259	192.91	-0.63	8.3	2.6	22.8	0.5
S129	99.06	7.40	0.4	0.13	-13.9	0.7	S263	194.59	-15.74	0.45	0.14	0.3	1.0
S132	102.96	-0.80	4.2	1.5	-48.5	1.5	S264	196.92	-10.37	0.4	0.13	12.0	0.5
S134	103.72	2.18	0.9	0.3	-16.1	0.5	S269	196.45	-1.68	3.8	1.0	17.5	0.7
S135	104.59	1.37	1.4	0.4	-20.7	0.5	S271	197.80	-2.33	4.8	0.5	20.5	0.5
S137	105.15	7.12	0.6	0.2	-10.3	1.4	S273	203.24	2.09	0.8	0.15	7.0	1.0
S139	105.77	-0.15	3.3	1.1	-46.5	0.5	S275	207.02	-1.82	1.6	0.2	14.3	0.1
S140	106.81	5.31	0.9	0.1	-8.5	1.0	S281	208.99	-19.39	0.5	0.05	8.0	1.5
S142	107.28	-0.90	3.4	0.3	-41.0	0.5	S283	210.81	-2.56	9.1	2.9	49.4	2.8
S149	108.34	-1.12	5.4	1.7	-53.1	1.3	S284	211.86	-1.18	5.2	0.8	45.0	0.7
S152	108.75	-0.93	3.6	1.1	-50.4	0.5	S285	213.81	0.61	6.9	0.7	45.3	1.1
S154	109.17	1.47	1.4	0.4	-11.5	0.9	S287	218.15	-0.35	3.2	0.8	27.2	0.8
S155	110.22	2.55	0.73	0.12	-10.0	1.5	S288	218.77	1.95	3.0	1.2	56.7	0.8
S156	110.11	0.05	6.4	2.0	-51.0	2.0	S292	224.10	-1.96	1.15	0.14	18.4	1.0
S157	111.28	-0.66	2.5	0.4	-43.0	2.0	S294	224.19	1.22	4.6	1.5	32.9	1.1
S158	111.54	0.78	2.8	0.9	-56.1	1.1	S299	230.97	1.49	4.4	0.6	47.6	0.4
S159	111.61	0.37	3.1	1.2	-56.0	1.0	S301	231.52	-4.33	5.8	0.9	53.0	0.4
S161B	111.89	0.88	2.8	0.9	-51.9	0.7	S302	232.63	1.01	2.2	0.7	16.6	0.3
S162	112.19	0.22	3.5	1.1	-44.7	0.5	S305	233.77	-0.15	5.2	1.4	44.1	0.6
S163	113.52	-0.57	2.3	0.7	-44.9	3.8	S307	234.57	0.83	2.2	0.5	46.3	0.7
S165	114.65	0.14	1.6	0.5	-33.0	1.0	S309	234.64	-0.21	5.5	0.8	44.0	1.7
S168	115.79	-1.65	3.8	1.2	-40.6	1.4	S310	239.65	-4.94	1.5	0.5	22.3	1.0
S170	117.57	2.26	2.3	0.7	-43.7	1.0	S311	243.20	0.44	4.1	0.6	51.0	1.6
S173	119.40	-0.84	2.7	0.9	-34.5	2.8	BFS54	211.27	-0.35	8.7	2.8	21.4	0.5

Burton 1988). The data for the 150 H I data points are listed in Table 2. The uncertainties in the H II region and H I data and the relative weighting of the two data sets are discussed below.

b) *Derived Quantities and Error Analysis*

i) *Basic Equations and Uncertainties*

A rotation curve can be shown as a plot of either w, the angular velocity, or Θ, the circular velocity, versus galactocentric radius R. The galactocentric radius is computed from

$$R = (R_0^2 + d^2 - 2R_0 d \cos l)^{1/2} , \quad (2)$$

where R_0 is the galactocentric distance of the Sun, d is the distance from the Sun to the object, and l is the galactic longitude of the object. For an object in circular rotation about the center of the Galaxy

$$\omega = \frac{V_r}{R_0 \sin l \cos b} + \omega_0 , \quad (3)$$

where V_r is the observed radial velocity, b is the galactic latitude, and ω_0 is the angular velocity of the Sun's rotation around the Galaxy. Equation (3) does not depend on R, so the value of ω is independent of R, unlike the value of $\Theta\,(= R\omega)$. A fit of ω versus R is a fit of two observationally independent quantities. In external galaxies Θ and R are measured directly and are the observationally independent quantities. In order to allow comparison with those rotation curves the rotation curves derived for our Galaxy are also displayed as Θ versus R curves. However, *all the Galactic rotation curves in this paper were fitted in ω versus R.*

For a Galaxy in circular rotation objects observed toward the galactic center and anticenter have no net V_r relative to the local standard of rest (LSR). In these directions all objects should be, on average, at a radial velocity of 0 km s^{-1}. However, examination of the data indicates that objects toward the galactic center tend to have positive radial velocities while those in the anti-center direction have negative radial velocities. The expected velocities of those objects that have optically determined distances were computed from a simple rotation curve model. The velocity residuals were then used to compute a radial velocity of the LSR 4.2 ± 1.5 km s^{-1}.

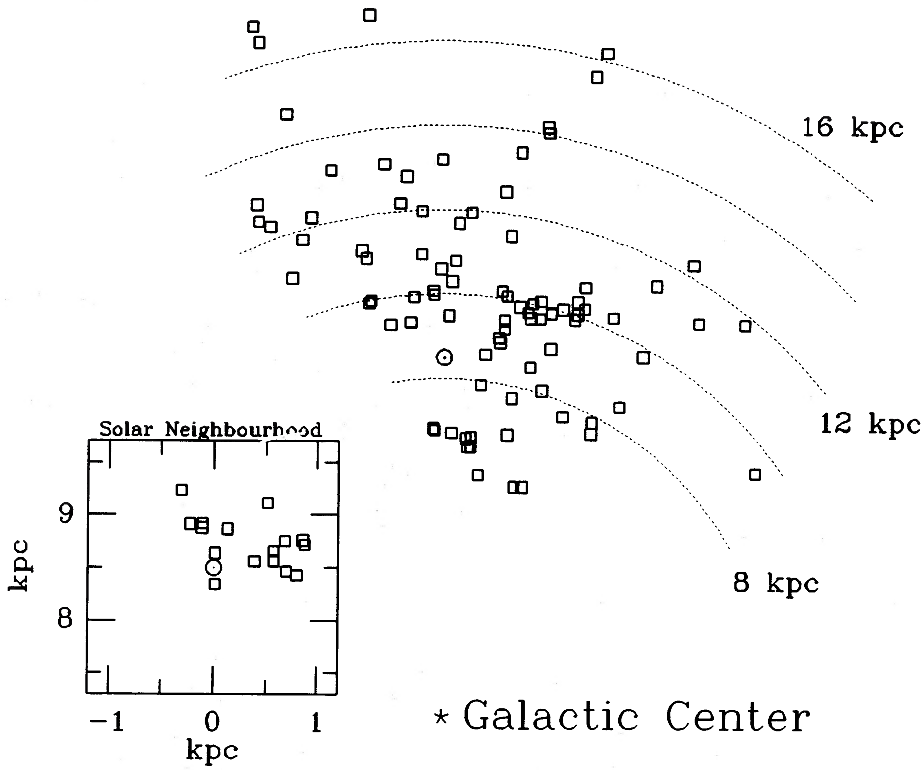

FIG. 1.—The positions of the H II regions used to determine the rotation curve. The H II regions within 1 kpc of the Sun are shown as an insert at the bottom left. The Sun's position is indicated with a "$\odot$."

We therefore correct for this effect by modifying equation (3) as follows:

$$\omega = \frac{V_r}{R_0 \sin l \cos b} + \omega_0 - \frac{V_\Pi \cos l}{R_0 \sin l}, \tag{4}$$

where $V_\Pi = 4.2$ km s^{-1}. For most objects this correction term is not significant.

The uncertainties in ω, σ_ω are computed from

$$\frac{\sigma_\omega^2}{(\omega - \omega_0)^2} = \frac{\sigma_{V_r}^2}{V_r^2} + \frac{\sigma_l^2}{\tan^2 l}, \tag{5}$$

where σ_{V_r} is the uncertainty in the radial velocity and σ_l is the uncertainty in the galactic longitude. The uncertainties in R, σ_R, are determined from

$$R^2\sigma_R^2 = (d - R_0 \cos l)^2\sigma_d^2 + (R_0 d \sin l)^2\sigma_l^2, \tag{6}$$

where σ_d is the uncertainty in the distance to the object. The actual quantities used in the fits were dimensionless versions of R and ω. These are

$$x \equiv \frac{R}{R_0} \tag{7}$$

and

$$y \equiv \frac{\omega - \omega_0}{\omega_0}. \tag{8}$$

The uncertainties in these quantities are then

$$\sigma_x = \frac{\sigma_R}{R_0} \tag{9}$$

and

$$\sigma_y = \frac{\sigma_\omega}{\omega_0}. \tag{10}$$

The measurement uncertainty in the radial velocity of the H II regions is always small, usually less than 1 km s^{-1}. A much larger contribution to this term is due to the presence of random motions of the complexes. We include a random velocity of 6.4 km s^{-1} added in quadrature to σ_{V_r} for each object. This value is derived from the analysis of the motions of center and anticenter complexes and is consistent with the velocity dispersion of $6.6^{+0.9}_{-0.6}$ km s^{-1} determined by Stark (1984). The uncertainties we use for the H I velocity data come entirely from the H I velocity dispersion of 4.5 km s^{-1} determined by Burton and Gordon (1978) from their data. We calculate the uncertainty in the H I distances (R) from R_0 and the spacing between the data points.

ii) *Results*

We present the data in two ways: as individual data points in Figure 2 and with data points averaged together in Figure 3. In Figure 2*a* we plot the data points in ω versus R and give error bars for a few of the H II regions that appear to be outliers and have the largest error bars. The error bars for H II regions near the center of the distribution (i.e., near R_0, ω_0) are smaller than the symbol used to plot the objects except if they lie near the center or anticenter direction or if they are close to the Sun ($d < 1$ kpc). One of the leftmost H II points is shown plotted with its error bars as well. The H I error bars are all smaller than the symbol used to plot the H I points. The two rows of data for the H I points result from the well known discrepancy in the northerm and southern hemisphere data.

TABLE 2

H I DATA

l (°)	V_r (km s^{-1})	l (°)	V_r (km s^{-1})	l (°)	V_r (km s^{-1})	l (°)	V_r (km s^{-1})
15	149.3	53	62.8	271	−0.1	309	−58.0
16	140.3	54	54.3	272	−0.2	310	−60.0
17	132.1	55	45.6	273	−0.8	311	−62.3
18	129.3	56	45.4	274	−0.5	312	−60.7
19	124.8	57	40.0	275	−3.8	313	−60.0
20	123.3	58	39.9	276	−3.2	314	−61.2
21	121.0	59	38.8	277	−3.6	315	−62.5
22	115.3	60	36.2	278	−5.9	316	−60.7
23	115.0	61	33.5	279	−4.6	317	−61.2
24	136.5	62	30.7	280	−5.6	318	−62.0
25	132.3	63	40.9	281	−6.3	319	−69.7
26	112.5	64	25.6	282	−8.8	320	−72.5
27	106.4	65	24.9	283	−10.7	321	−77.0
28	105.7	66	20.3	284	−12.6	322	−79.5
29	105.9	67	24.1	285	−14.8	323	−83.7
30	108.7	68	15.2	286	−17.5	324	−83.0
31	132.3	69	16.4	287	−15.9	325	−89.7
32	107.0	70	14.1	288	−15.9	326	−91.9
33	103.8	71	11.8	289	−16.8	327	−96.4
34	102.4	72	11.5	290	−10.0	328	−103.1
35	96.6	73	11.3	291	−18.3	329	−127.1
36	89.0	74	9.8	292	−21.2	330	−124.5
37	89.0	75	8.1	293	−22.7	331	−127.5
38	88.0	76	9.6	294	−24.3	332	−125.9
39	86.4	77	9.2	295	−25.2	333	−110.4
40	77.3	78	13.2	296	−28.8	334	−112.4
41	76.2	79	15.4	297	−33.2	335	−117.8
42	72.1	80	12.2	298	−33.7	336	−124.8
43	74.2	81	13.1	299	−30.7	337	−125.1
44	69.5	82	15.1	300	−35.4	338	−123.0
45	67.4	83	27.0	301	−39.4	339	−127.5
46	66.2	84	36.6	302	−41.6	340	−128.4
47	67.6	85	9.8	303	−45.5	341	−133.8
48	67.6	86	10.9	304	−45.5	342	−138.0
49	66.7	87	9.0	305	−44.9	343	−149.9
50	65.4	88	11.9	306	−41.0	344	−149.5
51	63.7	89	9.7	307	−48.6	345	−160.3
52	63.1			308	−56.0		

The relatively large uncertainty in the CO data comes from the uncertainties in the distances as well as from streaming and random motions of the complexes. Note in particular that the H II regions at large R have much larger uncertainties in the R direction than in the ω direction showing the effect of the distance uncertainties. Figure 2*b* shows the H I and CO data plotted in Θ versus R with error bars plotted for the same objects as in Figure 2*a*. Also shown in Figure 2 are fits discussed in § II*c*(ii).

Many of the H II regions in the range of $R = 9 \rightarrow 13$ kpc lie below the trend. Most of these objects are in the Perseus spiral arm. It has long been known that (see Münch 1957) young objects in the Perseus arm show a ~ 10 km s^{-1} velocity anomaly which is usually attributed to streaming motions. This decreases the computed value of ω for all of them.

Figure 3 shows the H I and CO data in 1 kpc bins. The points are the weighted means for all of the objects in a bin (H I and CO data plotted separately) where the weights include measurement uncertainties and the measured velocity dispersion. The error bars give the weighted uncertainty in the mean for each bin.

In both Figures 2 and 3 $R_0 = 8.5$ kpc and $\Theta_0 = 220$ km s^{-1}. From Figures 2 and 3 it is clear that over the entire range of R, Θ does not deviate from Θ_0 by more than 30 km s^{-1} or 14%. The curve is a flat or at most gently rising to $2R_0$.

c) Fitting of Functions

i) *Functions and Methodology*

We looked at many different functional forms:

$$y = a_1 + a_2 x + a_3 x^2 + \cdots , \tag{11}$$

$$y = \frac{a_1}{x} + a_2 - 1 , \tag{12}$$

$$y = \frac{a_1}{x^2} + \frac{a_2}{x} + a_3 + a_4 x + \cdots , \tag{13}$$

$$y = a_1 + a_2 e^{a_3 x} + a_4 e^{a_5 x^2} + \cdots , \tag{14}$$

$$y = e^{(a_1 + a_2 x a_3 x^2 + \cdots)} - 1 , \tag{15}$$

$$y = a_1 x^{a_2 - 1} + a_3 , \tag{16}$$

$$y = a_1 x^{a_2 - 1} + \frac{a_3}{x} - 1 , \tag{17}$$

$$y = a_1 x^{a_2} + a_3 x^{a_4} - 1 . \tag{18}$$

After fitting, some of the curves could be rejected by eye as giving significantly bad fits. In particular, we did not find any advantage to fitting any function involving many terms of a polynomial form (i.e., eqs. [11], [13], or [15]). These functions

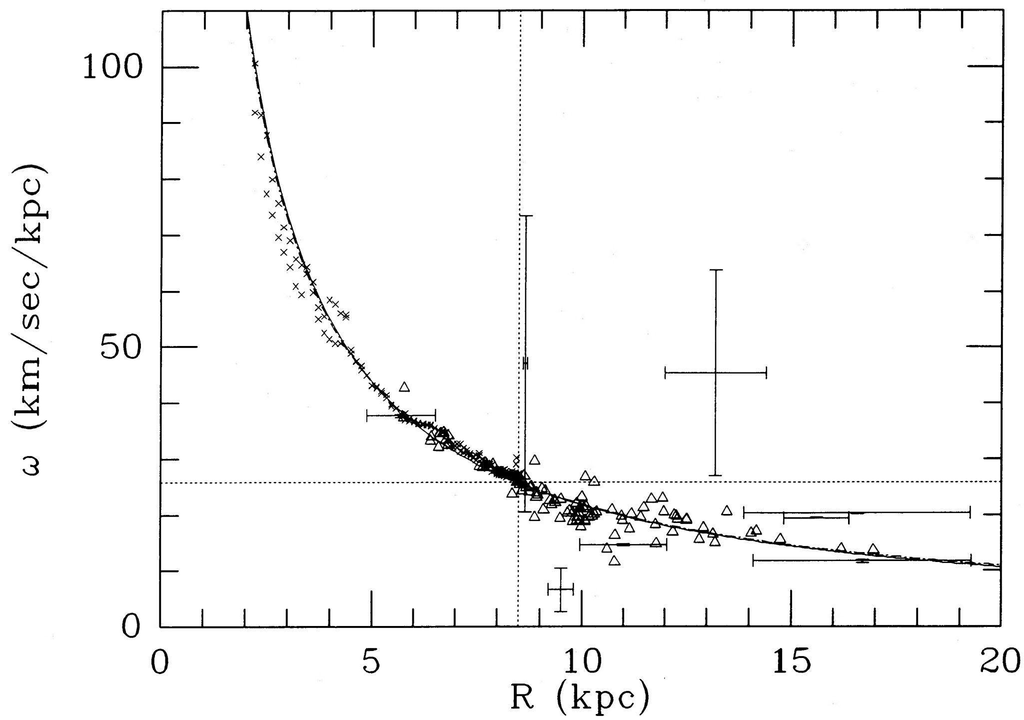

FIG. 2*a*

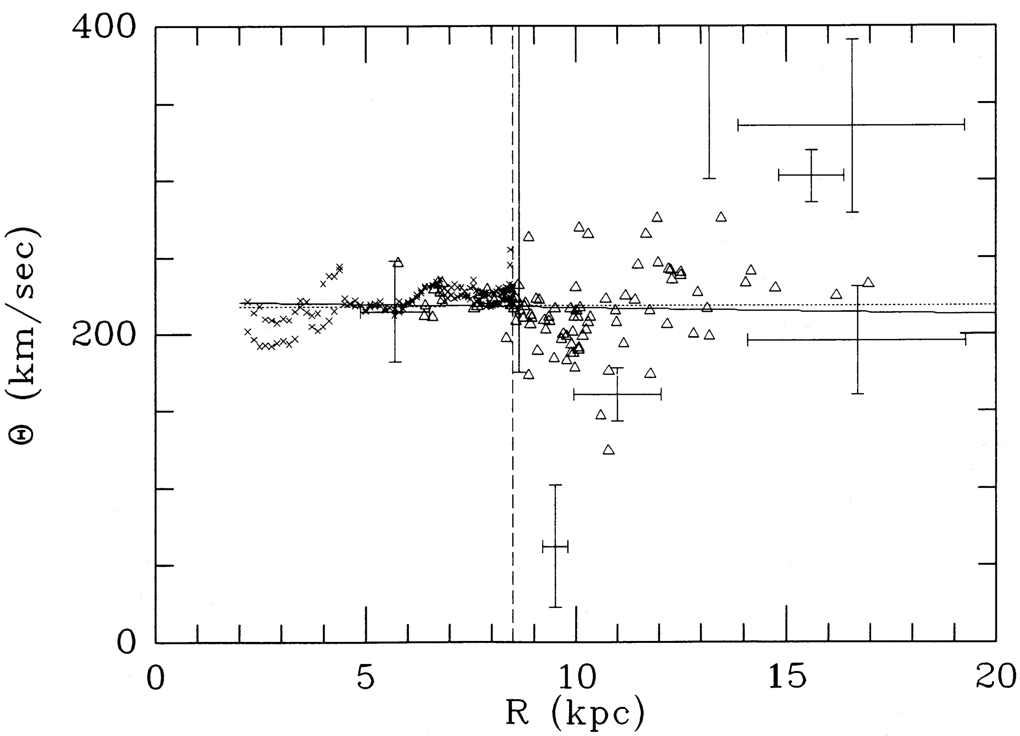

FIG. 2*b*

FIG. 2.—The data points used for the rotation curve determinations (*crosses* from H I rangent point data, *triangles* from CO data). Error bars are shown for a few outlying H II regions. Error bars for H II regions near the center of the distribution and for the H I points are in general smaller than the symbols used to plot the positions. (*a*) ω vs. R plot. (*b*) Θ vs. R plot. We show error bars for a few of the most uncertain CO data points. The "best-fit" linear (*solid line*) and power law (*dashed line*) rotation curves for the IAU standard values of $R_0 = 8.5$ kpc and $\Theta_0 = 220$ km s^{-1} are shown.

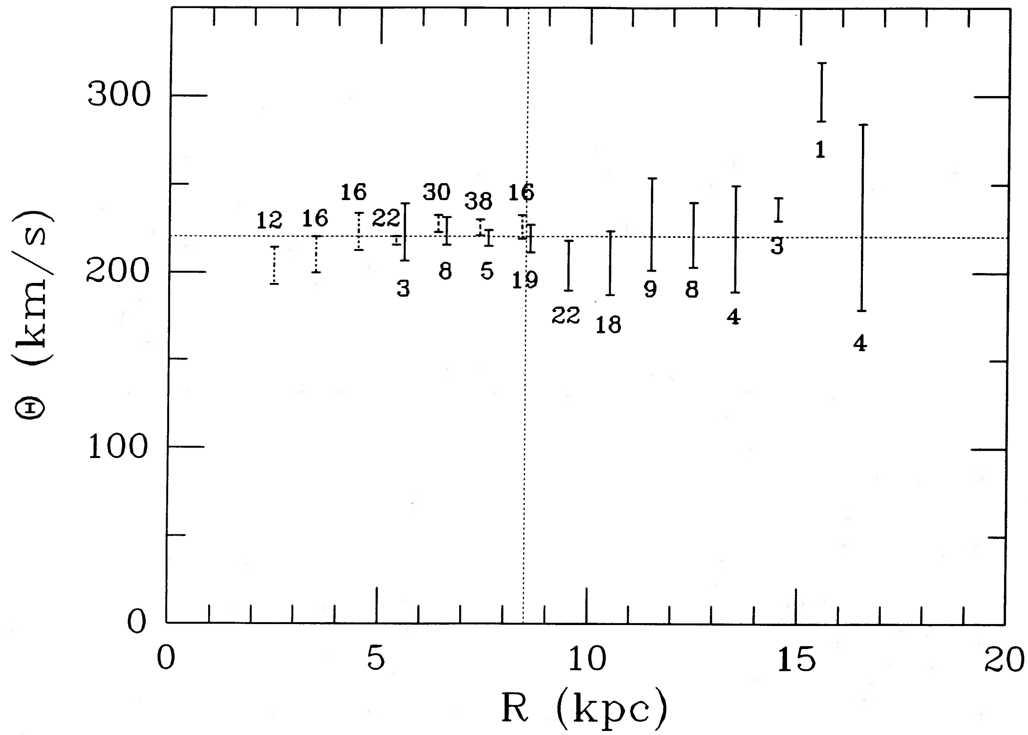

FIG. 3.—The H I and CO data binned in 1 kpc intervals in R. The values plotted are the mean Θ weighted by the uncertainties in the values of Θ for individual objects. The error bars give the weighted uncertainty in the mean for each bin.

tended to be very poorly behaved near the endpoints of the data.

Because the dip in Figures 2 and 3 at 10 kpc comes primarily from objects in the Perseus arm it is clear that at least some of the structure in the points are the result of streaming and not the result of large-scale mass distribution of the Milky Way. Therefore finding functions that reproduce the "wiggles" in the data will neither improve mass models nor produce more accurate kinematic distances in regions away from the objects used to determine the fit. We therefore limit our discussion to two simple functional forms that adequately describe the data: equation (12) corresponds to the simple linear rotation curve

$$\Theta = a_1 \Theta_0 + a_2 \omega_0 R \qquad (19)$$

and equation (17) corresponds to the simple power-law rotation curve

$$\Theta = \Theta_0 \left[a_1 \left(\frac{R}{R_0} \right)^{a_2} + a_3 \right], \qquad (20)$$

where the coefficients a_1 and a_2 in equation (19) are the same as those in equation (12) and the coefficients in equation (20) are the same as those in equation (17).

We determine a quantitative rotation curve by fitting a smooth curve (one of the above functions) to these data but, unlike most curve fit problems, there are significant uncertainties in both coordinates. We therefore fit the data using a "two-dimensional" reduced χ^2 fitting procedure described in the Appendix. The data were fitted in the ω versus R domain since these variables are more directly related to the observed quantities, and the error in ω is uncorrelated with errors in R, whereas errors in Θ are correlated with errors in R. To arrive at the actual rotation velocity (Θ, in km s^{-1}) ω is multiplied by R. The uncertainty in any measure of Θ is therefore a compound of the uncertainties both in the measured distance and in the radial velocity.

In all of these functions there exists a correlation between the coefficients of the functions. For example in equation (17), a_1 and a_3 always approximately sum to unity because $y \approx 0$ (i.e., $\omega \approx \omega_0$), where $x = 1$ (i.e., $R = R_0$). Since a_1 and a_2 determine the slope of the curve at $x = 1$ there must also be a dependence between a_1 and a_2. This effect is illustrated by the values in Table 3 where the coefficients for four essentially identical curves are given. These represent the best fits with identical data and identical rotation parameters but with different "initial guesses" for the values of the coefficients. Again, these values produce curves that are essentially identical, both in appearance and in the significance of their fit to the data.

The rotation curve fitting routine was subjected to a number of convergence tests. Various starting conditions, convergence intervals, and stopping criteria were used. It was found that the routine was very stable, converging to the same unique solution for a given data set independent of the starting criteria, if the routine was given sufficient time to allow convergence. The stopping criteria was an insignificant improvement in χ_ν^2 with successive iterations.

One of the test performed on the fitting procedure was to restrict the data set to exclude all objects within some radius

TABLE 3

COEFFICIENTS OF EQUATION (16) THAT PRODUCE INDISTINGUISHABLE ROTATION CURVES

COEFFICIENT	CURVE			
a_1	0.310	0.419	0.512	0.603
a_2	0.169	0.124	0.109	0.094
a_3	0.688	0.584	0.493	0.402

centered on the Sun. Objects near the Sun will have small circular velocities and therefore any noncircular component to their velocity will have a larger relative effect on the value of ω. We found that there was a small but measurable difference in the fits for different distance limits. For all fits described here objects within 1 kpc of the Sun have been excluded.

Other restricted data sets used in the fits performed as expected. The H I data points were removed and the resultant rotation curve (Θ vs. R) was steeper, rising more rapidly. Using longitude subsets of the data (e.g., only objects $l = 0°$ $l = 150°$) produced no significant differences.

The last test was to increase the optical distances determined for all objects by 25% to simulate a systematic error in those measurements. This increased the slope of the resultant rotation curve fits. The amount of the increase depends on the exact choice of parameters but was less than 1 km s^{-1} in Θ versus R.

ii) *Results*

Figures 2*a* and 2*b* show the "best fit" rotation curves for the new IAU standard values for R_0 and Θ_0 of 8.5 kpc and 220 km s^{-1}. The linear fit shown is the function

$$\frac{\omega}{\omega_0} = 1.00746\left(\frac{R_0}{R}\right) - 0.017112 \tag{21}$$

and the power-law fit shown is

$$\frac{\omega}{\omega_0} = 0.49627\left(\frac{R_0}{R}\right)^{0.99579} + 0.49632\left(\frac{R_0}{R}\right). \tag{22}$$

These correspond to Θ rotation curves

$$\Theta = (221.641 - 0.44286R) \text{ km s}^{-1} \tag{23}$$

and

$$\Theta = (109.190 + 108.201R^{0.0042069}) \text{ km s}^{-1}, \tag{24}$$

where R is in kpc.

These curves are nearly identically flat, Θ changing by less than 2% from R_0 to $2R_0$. As pointed out earlier, near $R = 10$ kpc a great many of the H II regions fall well below the derived rotation curve while at $R \geq 12$ kpc roughly $\frac{3}{4}$ of the H II regions are above the curve. It should also be noted that both functions, while very different in form, produced very similar best-fit rotation curves.

Table 4 lists the rotation curve coefficients for a variety of representative values of the rotation parameters. The Oort A constant is given, as defined by

$$A \equiv -\frac{R_0}{2}\left(\frac{d\omega}{dR}\right)_{R_0}. \tag{25}$$

It should be emphasized that this value of A is based on a global data set rather than on objects near the Sun as it is usually measured. Thus the values found here do not necessarily agree with the local value. The values of the Oort A coefficient from the fits are very weakly dependent on Θ_0 and decrease linearly with increasing R_0. The slope of the result Θ versus R curve at R_0 is also given in Table 4.

Figure 4 is an attempt to represent the entire range of acceptable fits. It shows the most steeply rising and most rapidly declining rotation curves found in the fits, all plotted on a scaled plot of Θ/Θ_0 versus R/R_0.

Figure 5*a* is a representation of the size of the velocity residuals

$$V_r(\text{residual}) = V_r(\text{observed}) - V_r(\text{expected from fit}) \tag{26}$$

TABLE 4

ROTATION CURVE FITS FOR VARIOUS ROTATION PARAMETERS

R_0 (kpc)	ω_0 (km s^{-1} kpc^{-1})	Θ_0 (km s^{-1})	a_1	a_2	a_3	A (km s^{-1} kpc^{-1})	Slope at R_0 (km s^{-1} kpc^{-1})
			Power Law				
8.5..........	25.88	220	0.49627	0.0042069	0.49632	12.82	0.054
5.0..........	44.00	220	0.53305	0.22980	0.50279	20.09	5.39
6.0..........	36.67	220	0.51202	0.13204	0.50548	17.41	2.48
7.0..........	31.43	220	0.50406	0.063417	0.50171	15.30	1.01
8.0..........	27.50	220	0.49915	0.029419	0.49958	13.53	0.40
9.0..........	24.44	220	0.49491	−0.0064658	0.49494	12.14	−0.08
10.0..........	22.00	220	0.49141	−0.034475	0.49131	11.00	−0.37
5.0..........	36.00	180	0.51162	−0.80006	0.52019	19.31	−1.47
5.0..........	50.00	250	0.58119	0.37710	0.45267	20.37	10.96
10.0..........	18.00	180	0.49986	−0.29428	0.47695	10.12	−2.65
10.0..........	25.00	250	0.51315	0.13514	0.47254	11.45	1.73
			Linear				
8.5..........	25.88	220	0.97800	0.025255	...	12.66	0.65
5.0..........	44.00	220	0.87829	0.15227	...	19.32	6.70
6.0..........	36.67	220	0.93032	0.084250	...	17.05	3.09
7.0..........	31.43	220	0.97023	0.033675	...	15.25	1.06
8.0..........	27.50	220	0.99334	0.0030385	...	13.66	0.08
9.0..........	24.44	220	1.01697	−0.029742	...	12.41	−0.73
10.0..........	22.00	220	1.03257	−0.052868	...	11.36	−1.16
5.0..........	36.00	180	1.07158	−0.35345	...	19.29	−1.27
5.0..........	50.00	250	0.77698	0.25058	...	19.53	12.53
10.0..........	18.00	180	1.26249	−0.28761	...	11.36	−5.18
10.0..........	25.00	250	0.90807	0.074216	...	11.35	1.86

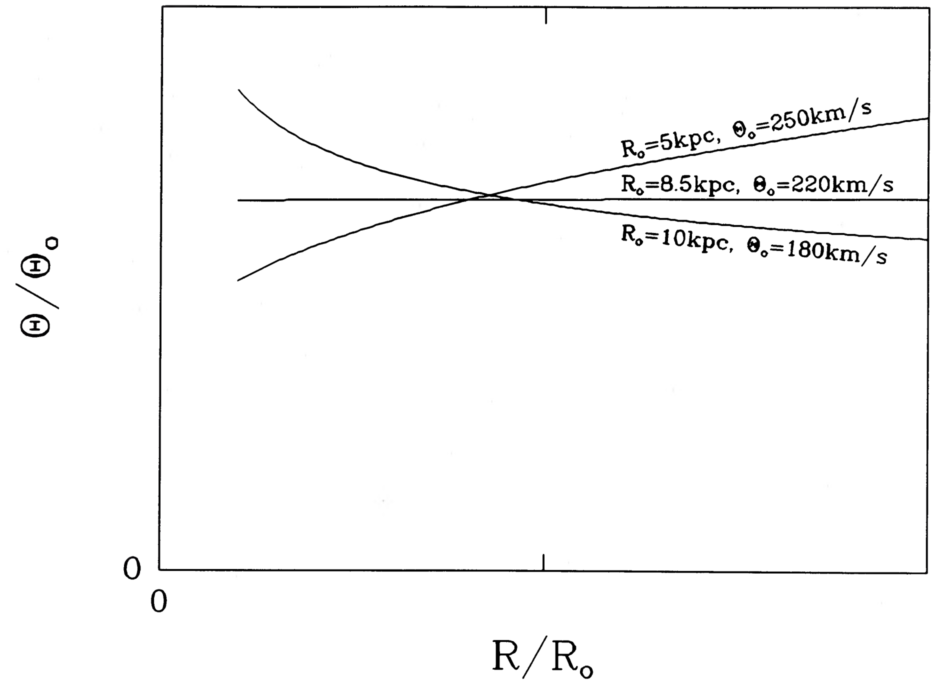

FIG. 4.—Plots of the "best-fit" power-law rotation curves scaled by R_0 and Θ_0

for the individual objects plotted as a function of galactocentric distance. The best fit power-law function and the standard values of R_0 and Θ_0 (8.5 kpc, 220 km s^{-1}) were used to calculate the residuals. The velocity residuals are plotted on the galactic plane in the positions of the objects in Figure 5*b* with different symbols representing positive or negative residuals and the size symbol proportional to the magnitude of the residual. Both of these plots show the presence of significant noncircular motions, especially in the Perseus arm.

Figure 6 shows the goodness-of-fit parameter χ^2_ν for many of the fits plotted against the values of R_0 and ω_0 used for the fits. There are surprising minima in the global best-fit for both functions, regardless of the R_0 and Θ_0 used to generate the fits, at values of $R_0 \approx 6.2$ kpc and $\omega_0 \approx 33$ km s^{-1} kpc^{-1}.

III. DISCUSSION

The most important factor in answering the question "Does the rotation curve rise?" is the combination of the values of the rotation parameters R_0 and Θ_0. With the "old" IAU values of $R_0 = 10$ kpc and $\Theta_0 = 250$ km s^{-1} the best fits show a rise of the order of 20 km s^{-1} from R_0 to $2R_0$. The current IAU values of $R_0 = 8.5$ kpc and $\Theta_0 = 220$ km s^{-1} produce flat rotation curve fits. The general rule is that larger values of R_0 cause the rotation curve slope to decline while larger values of Θ_0 increases the slope and, a fractional change in Θ_0 is more effective in changing the slope than a fractional change in R_0 (see Shuter 1981).

As shown in the results (§ II*c*[ii]), the best fit rotation curves are insignificantly different from a flat rotation curve for values of R_0 near 8.5 kpc and Θ_0 near 220 km s^{-1}. However, if we average the eight outermost points together then they collectively lie above the mean curve by 2.5 σ. The answer to the question "Does the rotation curve rise ?" depends on how one defines the question. The mean curve defined by all of the data points does not but the trend of points beyond $1.5R_0$ does allow the possibility of a rise by $\sim$30 km s^{-1} at the 2.5 σ level (for $R_0 = 8.5$ kpc and $\Theta_0 = 220$ km s^{-1}). Furthermore Moffat (1988) has recently found a distance of 10.0 kpc and a velocity of 47.7 km s^{-1} for S289, which for the standard R_0 and Θ_0 implies a circular velocity of 298 $\pm$ 33 at $R = 17.5$ kpc, consistent with an even steeper rise in the rotation curve.

The rise in the rotation curve apparent in the data we are analyzing has been recently reevaluated by Hron (1988), who has looked at the question of how metallicity effects might cause systematic errors in the stellar distances. He finds that at $2R_0$, the calculated value of Θ_0 is overestimated by 15% for a metallicity gradient of $\log Z/Z_0 = 0.1$ kpc^{-1}, where Z is the heavy element abundance. If the actual metallicity gradient in the outer Galaxy is this large, the effect would be to make the outermost points in Figure 3 lie very close to an identically flat rotation curve. If the metallicity gradient is half of this value, then one still finds that the outermost points lie above the mean curve, but the significance of the rise is decreased.

The metallicity correction, therefore, has the effect of bringing the outermost points closer to an identically flat curve. However, since the metallicity gradient in the outer part of the Milky Way at large galactocentric distances is poorly known, it is unclear what the magnitude of the effect is (see Hron 1988 for a discussion of this point). However, since the number of data points involved is small, and they carry relatively little weight, the effect of metallicity on the functions given in Table 4 should be negligible.

a) Comparison with Other Work

The principal method of measuring the rotation curve in our Galaxy has been the "H I tangent point method," where H I inside the solar circle is used to derive the *inner Galaxy* rotation curve (e.g., Burton and Gordon 1978). Knapp, Tremaine, and Gunn (1978) looked at H I near $l = 90°$ and various models of the radial distribution of H I to show that the data are most consistent with a flat rotation curve, an exponentially decreasing H I density, and a rotation rate of $\theta = 220$ km s^{-1}.

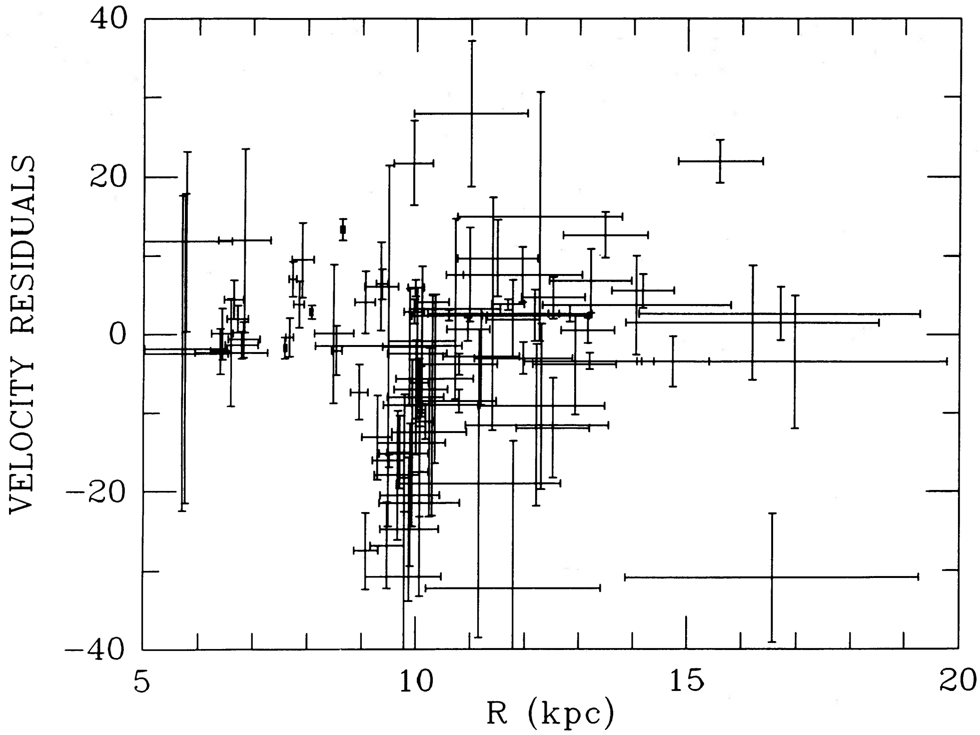

FIG. 5*a*

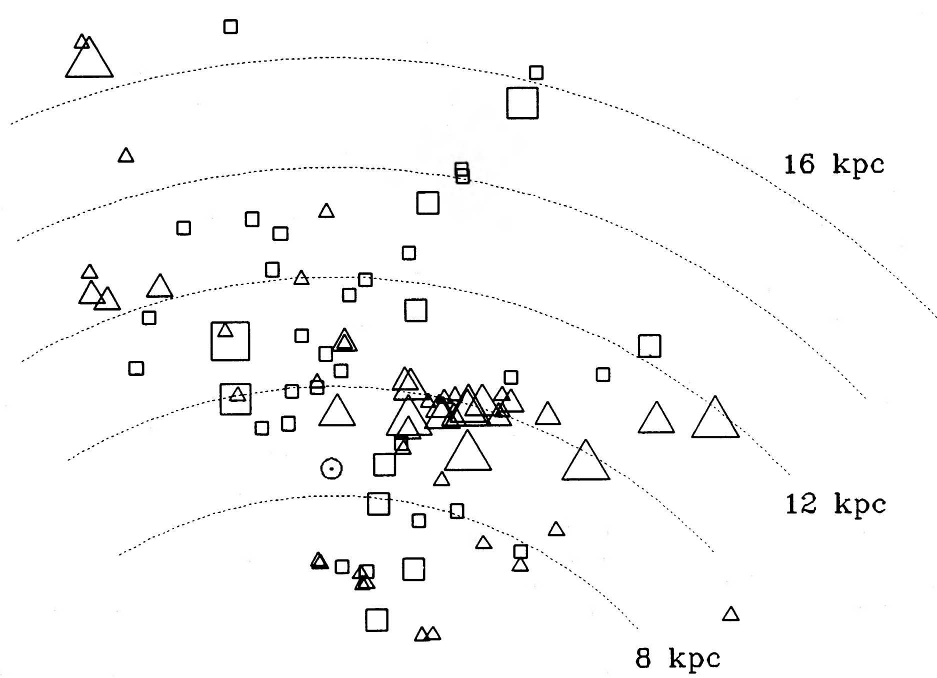

FIG. 5*b*

FIG. 5.—The velocity residuals for the individual H II regions. Shown as V_r(observed) − V_r(expected from fit) (power-law model). (*a*) Plotted vs. *R*. (*b*) Plotted in projection on the galactic plane. The size of the symbol indicates the size of the residual. An open square indicates a positive residual, a triangle indicates a negative residual. The Sun's position is indicated with a "⊙."

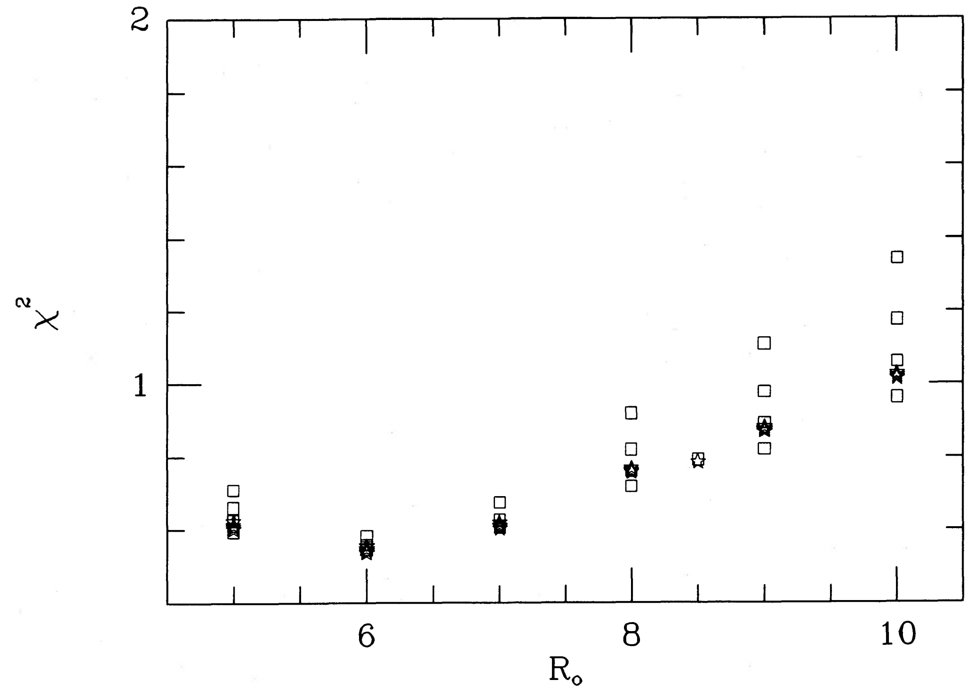

FIG. 6*a*

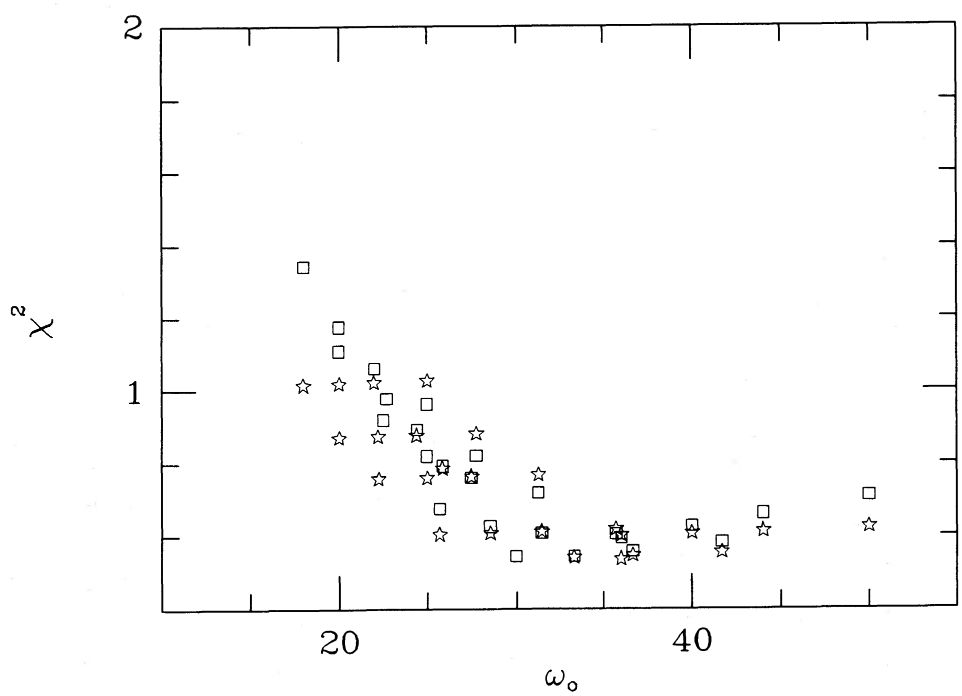

FIG. 6*b*

FIG. 6.—The goodness-of-fit parameter χ_ν^2 is plotted against (*a*) the value of R_0 used for the fit and (*b*) the value of ω_0 used for the fit. The linear rotation curve model is shown as stars and the power-law model is shown as open squares. Each plotted point represents the χ_ν^2 of the given value of R_0 or ω_0 for a best fit for some value of Θ_0. The origin of the minima is not understood.

Hartwick and Sargent (1978) used distant galactic globular clusters and companion galaxies to show that the mass of the Galaxy at 3.4 to $7.6 \times 10^{11}\ M_{\odot}$ is 2–4 times greater than previously thought, implying that the rotation curve does not fall at very large distances from the center. Little and Tremaine (1988) have also analyzed the Milky Way companion galaxies and have found that the mass of the Galaxy is $2\text{–}5 \times 10^{11}\ M_{\odot}$.

All methods of obtaining the *outer* Galaxy rotation curve have one thing in common: the independent measurement of distances and velocities of a suitably selected group of objects. These include star clusters (Moffat, FitzGerald, and Jackson 1981), H II regions/molecular clouds (this work; Chini and Wink 1984; Brand 1986), planetary nebulae (Schneider and Terzian 1983), carbon stars (Schechter *et al.* 1988), Cepheid values (Welch 1988), and the atomic hydrogen (Petrovskaya and Teerikorpi 1986). In general, the agreement between these determinations is good, with some differences evident at the 10%–15% level. The various methods are discussed in detail below. Comparisons are made using the same R_0 and Θ_0.

i) *Star Clusters*

The fundamental distance determinations of Moffat, FitzGerald, and Jackson (1981) have been central for measuring the rotation curve to large R. Because the brightest cluster members also excite H II regions and reflection nebulae, the distances determined to the clusters are also important for the H II region/molecular cloud method. The basic results were published in Jackson, FitzGerald, and Moffat (1978) who show a rotation curve (plotted as $R - R_0$ against $\omega - \omega_0$) that shows most of the points beyond $R - R_0 = 4$ kpc lying above a flat curve in Θ versus R, consistent with what is seen in Figure 2.

ii) H II *Regions/Molecular Clouds*

The first systematic work using H II regions to measure the outer Galaxy rotation curve used Hα velocities and the distances to the stars exciting the optical nebulae (Georgelin 1975; Georgelin and Georgelin 1976). This technique made it possible to determine the rotation curve to $1.3R_0$, not quite far enough to be convincingly different from the Schmidt (1965) model. Nevertheless, the rotation curve is flat to the last measured point.

The first paper using CO velocities of molecular clouds associated with H II regions to obtain the rotation curve to large R showed that the most distant points tended to lie above a flat curve (Blitz 1979). The significance of the rise was not clear, however, because of the relatively few data points. Subsequent work (Blitz, Fich, and Stark 1980; BFS) demonstrated the persistence of the rise in the outermost points, although the value of the rotation constants can significantly affect the shape of the curve (Blitz and Fich 1983).

Chini and Wink (1984) obtained distances and velocities to 15 distant H II regions and found an even steeper rise in the data than Blitz, Fich, and Stark (1980). They determined velocities from radio recombination lines, a method which gives unbiased velocities (Fich, Treffers, and Blitz 1982), but cannot, of course, be used for distant reflection nebulae. Chini and Wink measured distances to seven objects previously observed by others, and although there is a large scatter, their distances are systematically high by 33% (4/3 higher, corrected downward in § II*a* by 25% to 3/4 of their original value). This difference induces a rise in the data; when all of their distances are corrected downward, the rise appears to be consistent with that shown in Figure 2.

The most recent measurements by Brand (1986) of objects in the southern hemisphere do not go to large enough distances to determine whether the rise at large R exists in the southern data. There are some detailed differences in the rotation curve which can be attributed to velocity streaming. These will be discussed in a subsequent paper (Brand and Blitz 1989).

Clemens (1985) has merged the BFS data with data from the Massachusetts-Stony Brook CO survey to attempt to obtain an overall CO rotation curve. His curve has far more structure, and the excursions from a flat curve are significantly larger than the curves shown in Figure 2. The reasons are as follows.

1. Clemens fits three polynomials separately, of order 5–7, in three distinct distance regimes. This introduces large excursions resulting from streaming motion such as is seen in the Perseus arm.

2. The data are not weighted in the fits. This introduces the inflection point near the Sun, because data near it are heavily weighted. In addition, to obtain a well behaved polynomial for the outer Galaxy data, Clemens anchored the rotation curve at large R by using one of the mass determinations of Hartwick and Sargent (1978) interior to $R = 6.7R_0$. The work of Little and Tremaine (1988) implies the value used by Clemens is a significant overestimate.

Because of these problems, use of the polynomials derived by Clemens may lead to significant errors in the determination of kinematic distances at various longitudes in the second and third galactic quadrants (see Brand 1986). In the inner Galaxy, however, the derived rotation curve deviates insignificantly from that of Burton and Gordon (1978).

iii) *Planetary Nebulae*

Schneider and Terzian (1983) used planetary nebulae to determine the rotation curve to large R. They did not derive a functional fit to their data, preferring instead a representation of the binned data similar to that shown in Figure 3. Their data show a rise with the binned data all lying above a flat curve at $R > 1.5R_0$. They do an error analysis and compare their data with the BFS data. The results show good agreement within 1.5 σ in each bin. Their data give somewhat higher rotational velocities than do ours, but the difference is not significant. If, however, a metallicity correction is required for the molecular cloud/H II region sample, then a similar correction to the Schneider and Terzian data would be required to maintain the good agreement between these two independent sets of results.

iv) H I

The work of Knapp, Tremaine, and Gunn (1978) was the first attempt to use the H I data beyond the solar circle to obtain information on the rotation curve to large R. Although they did not, strictly speaking, measure the rotation curve, these authors showed that consistency with the data is best achieved at large R if the rotation curve is flat. However, it was not possible to assess the uncertainties with this method (see Knapp 1988 for a recent rediscussion of this method of analysis). More recently, Rohlfs *et al.* (1986) used the Maryland-Green Bank H I survey (Westerhout and Wendland 1982) to do a new tangent point analysis of the inner Galaxy rotation as well as the BFS data set supplemented by Chini and Wink (1984) data. Although they find best values of $R_0 = 7.9$ kpc and $\Theta_0 = 184$ km s^{-1}, the rotation curve they find is not substantially different from ours in shape. This is probably due to the similar value of ω_0 used in Figure 3.

A fundamentally new technique was developed by Petrovskaya and Teerikorpi (1986) who found good agreement with Blitz (1979); their mean outer Galaxy rotation curve rises above a flat curve.

v) *Carbon Stars*

Recently, Schechter *et al.* (1988) have used carbon stars as a measure of the rotation curve for $R > R_0$. Like the planetary nebulae, the carbon stars are probing an evolved stellar population, and unlike the other methods, both planetary nebulae and carbon stars sample the rotation curve with ballistic particles. The results so far are preliminary, but the carbon stars yield a flat rotation curve for $R < 1.5R_0$. Beyond that distance, all of the data are binned into a single point, which is necessary because errors for any individual star are much larger than for the objects used in this paper. That single point lies above a flat rotation curve. There does not appear to be a significant difference between the Schechter *et al.* result and ours, but a detailed comparison awaits the publication of their data.

Considerably more data are available than have been analyzed to date (P. Schechter, personal communication). The data currently reduced are in a narrow range of galactic longitude more southerly than any of the objects in our study. These carbon star data should ultimately provide a good test of any small rise in the rotation curve at large R.

vi) *Rotation of Other Galaxies*

Although the rotation of a few other galaxies had been measured in the past (see Burbidge and Burbidge 1975 for a review of this early work) large systematic rotation curve surveys have only recently been undertaken. Rubin (1983) describes a number of systematic properties of the rotation of galaxies as observed from the emission lines of the H II regions contained within them. One of these properties is particularly relevant to the work discussed in this paper: "virtually all rotation curves continue to rise with distance from the nucleus" with a slight rise that is in the mean between $V \propto R^{0.1}$ to $V \propto R^{0.2}$ for both Sb's and Sc's.

The rotation curves in H I described by Bosma (1983) extend to about twice the distance from the nucleus as the H II region rotation curves. Although there may be some evidence of falling rotation curves at large galactocentric distances in a few galaxies, in general the H I rotation curves are also slightly rising or flat in the great majority of cases.

vii) *Comparison Summary*

All nine of the above methods for determining the rotation curve to large R show that the rotation curve does not fall out to the last measured point, at a distance (generally) near $2R_0$. These results indicate that beyond $\sim 1.5R_0$, the mean of binned points lie above a flat rotation curve by $\sim$10%–20% of the circular velocity. However, metallicity effects could lower the extent to which the points lie above a flat curve for several of the data sets. Insofar as it is possible to intercompare the results (given the absence of error analysis in many cases), the rotation curves for all methods are in reasonable agreement with one another.

IV. RECOMMENDATIONS

The most common prescription for finding a kinematic distance to an object in the outer Galaxy is to "use a flat rotation curve." We stress here that this only gives even approximately correct values for a small range of rotation parameters (i.e., R_0, Θ_0). For example: using $R_0 = 8.5$ kpc and $\Theta_0 = 220$ km s^{-1} the difference between a kinematic distance computed with a flat curve, our best-fit linear curve, and our best-fit power-law curve is less than 10% over most of the outer Galaxy. Since the kinematic distance uncertainties will likely be on the order of 25% from other sources of error, it really does not matter which of these rotation curves is used.

We recommend that a flat rotation curve $\Theta = 220$ km s^{-1} be used for computing approximate kinematic distances with the IAU standard rotation parameters of $R_0 = 8.5$ kpc and $\Theta_0 = 220$ km s^{-1}.

If for some reason one should wish to depart from the IAU standard values of the rotation parameters then one should not in general invoke a flat rotation curve. We recommend that the linear best-fit curve appropriate to the desired rotation parameters be used for kinematic distance determinations. It is to be preferred over the power law function because it is simpler to use in calculations. Studies of the mass distribution of the Galaxy, however, are better served by using the power-law best-fit curves as they, in general, better represent the inner Galaxy H I data.

We thank W. B. Burton for providing the H I data. This work is partially supported by US NSF grant number AST86-18763.

APPENDIX

χ_ν^2 MODEL FITTING WITH UNCERTAINTIES IN TWO COORDINATES

The idea in measuring the reduced chi-squared (χ_ν^2) fit of some data to a model is that the square of the deviation, *in terms of the measurement uncertainty*, between data and model is summed for each measured point. The measurement is usually expressed as an ordered pair (x, y) where the value of x is well known while the value of y is uncertain by some amount σ_y. If the model is expressed by some function $f(x)$ then the χ_ν^2 is given by

$$\chi_\nu^2 \equiv \frac{\sum_{i=1}^{N}[(f(x_i) - y_i)^2/\sigma_{yi}^2]}{N - n - 1} , \tag{A1}$$

where N is the number of data points and n is number of degrees of freedom in the function $f(x)$. The deviation is weighted by the uncertainty in the measurement, but the only deviation between the data and the function is in the y direction.

Here we describe a simple extension of this technique for data in which there is an uncertainty in both the x and y measurements. The χ_ν^2 is described here by

$$\chi_\nu^2 \equiv \frac{\sum_{i=1}^{N}[(y_{ci} - y_i)^2/\sigma_{yi}^2] + [(x_{ci} - x_i)^2/\tau_{xi}^2]}{N - n - 1} , \tag{A2}$$

where (x_{ci}, y_{ci}) is the point on the curve describing the model that is "closest" to the data point (x_i, y_i). The point (x_{ci}, y_{ci}) is the one that minimizes the distance (r_i):

$$r_i = \frac{(y_{ci} - y_i)^2}{\sigma_{yi}^2} + \frac{(x_{ci} - x_i)^2}{\sigma_{xi}^2} . \quad \text{(A3)}$$

Thus the χ_ν^2 is the normalized sum of these closest distances r_i. Finding the points (x_{ci}, y_{ci}) is computationally equivalent to finding the roots of many equations and is computationally intensive. Varying the function changes the points (x_{ci}, y_{ci}), the distances r_i, and therefore the χ_ν^2. The function that gives the minimum value of χ_ν^2 is the "best fit" to the data. A more rigorous examination of this method has indicated that these χ_ν^2 values are not necessarily χ^2 distributed. This means that the actual numerical value of χ determined from this kind of analysis cannot be used for the usual sort of goodness of fit analysis.

The χ_ν^2 minimum was found through a gradient search technique described in Bevington (1969).

REFERENCES

Bevington, P. R. 1969, *Data Reduction and Error Analysis for the Physical Sciences* (McGraw-Hill).
Blitz, L. 1979, *Ap. J. (Letters)*, **231**, L115.
Blitz, L., and Fich, M. 1983, in *Astrophysics and Space Science*, Vol. **100**, *Kinematics, Dynamics, and Structure of the Milky Way*, ed. W. L. H. Shuter (Dordrecht: Reidel), p. 143.
Blitz, L., Fich, M., and Stark, A. A. 1980, *IAU Symposium 87, Interstellar Molecules*, ed. B. Andrew (Dordrecht: Reidel), p. 213.
———. 1982, *Ap. J. Suppl.*, **49**, 183 (BFS).
Bosma, A. 1983, *IAU Symposium 100, Internal Kinematics and Dynamics of Galaxies*, ed. E. Athanassoula (Dordrecht: Reidel), p. 11.
Brand, J. 1986, Ph.D. thesis, Leiden University.
Brand, J., and Blitz, L. 1989, in preparation.
Burton, W. B. 1988, *Trans, IAU*, **XXA**, 377.
Burton, W. B., and Gordon, M. A. 1978, *Astr. Ap.*, **63**, 7.
Burbidge, E. M., and Burbidge, G. R. 1975, in *Galaxies and the Universe*, ed. A. Sandage, M. Sandage, and J. Kristian (Chicago: University of Chicago Press), p. 81.
Chini, R., and Wink, J. E. 1984, *Astr. Ap.*, **139**, L5.
Clemens, D. P. 1985, *Ap. J.*, **295**, 422.
Fich, M., Treffers, R. R., and Blitz, L. 1982, in *Regions of Recent Star Formation*, ed. R. S. Roger and P. E. Dewdney (Dordrecht: Reidel), p. 201.
Forbes, D. G. 1985, Ph.D. thesis, University of Victoria.
Georgelin, Y. M. 1975, thesè de doctorat, Université de Provence.
Georgelin, Y. M., and Georgelin, Y. P. 1976, *Astr. Ap.*, **49**, 57.
Gunn, J. E., Knapp, G. R., and Tremaine. S. D. 1979, *A.J.*, **84**, 1181.
Hartwick, F. D. A., and Sargent, W. L. W. 1978, *Ap. J.*, **221**, 512.
Horn, J. 1988, *Astr. Ap.*, submitted.
Jackson, P. D., Fitzgerald, M. P., and Moffat, A. F. J. 1979, in *IAU Symposium 84, The Large-Scale Characteristics of The Galaxy*, ed. W. B. Butler (Dordrecht: Reidel), p. 221.
Knapp, G. R. 1988, in *The Outer Milky Way*, ed. L. Blitz and J. Lockman (New York: Springer), p. 3.
Knapp, G. R., Tremaine, S. D., and Gunn, J. E. 1978, *A.J.*, **83**, 1585.
Little, B., and Tremaine, S. 1987, *Ap. J.*, **320**, 493.
Moffat, A. F. J., Fitzgerald, M. P., and Jackson, P. D. 1979, *Astr. Ap. Suppl.*, **38**, 197.
Münch, G. 1957, *Ap. J.*, **125**, 42.
Petrovskaya, I. V., and Teerikorpi, P. 1986, *Astr. Ap.*, **163**, 39.
Rohlfs, K., Chini, R., Wink, J. E., and Böhme, R. 1986, *Astr. Ap.*, **158**, 181.
Rubin, V. C. 1983, in *IAU Symposium 100, Internal Kinematics and Dynamics of Galaxies*, ed. E. Athanassoula (Dordrecht: Reidel), p. 3.
Schechter, P., Aaronson, M., Cook, K. H., and Blanco, V. M. 1988, in *The Outer Galaxy*, ed. L. Blitz and J. Lockman (New York: Springer), p. 31.
Schmidt, M. 1965, in *Galactic Structure*, ed. A. Blaauw and M. Schmidt (Chicago University of Chicago Press), p. 513.
Schneider, S. E., and Terzian, Y. 1983, *Ap. J.*, **274**, L61.
Shuter, W. L. H. 1981, *M.N.R.A.S.*, **194**, 851.
Stark, A. A. 1984, *Ap. J.*, **281**, 624.
Welch, D. W. 1988, in *The Mass of the Galaxy*, ed. M. Fich (Toronto: CITA), p. 29.
Westerhout, G., and Wendland, H.-U. 1981, *Astr. Ap. Suppl.*, **49**, 137.

LEO BLITZ: Astronomy Program, University of Maryland, College Park, MD 20742

MICHEL FICH: Physics Department, University of Waterloo, Waterloo, Ontario N2L 3G1, Canada

ANTONY A. STARK: AT&T Bell Laboratories, Holmdel, NJ 07733